

Received July 31, 2020, accepted August 7, 2020, date of publication August 11, 2020, date of current version August 24, 2020.

Digital Object Identifier 10.1109/ACCESS.2020.3015715

A Review of Nonlinear Transmission Line System Design

ANDREW J. FAIRBANKS¹, (Graduate Student Member, IEEE),
ADAM M. DARR¹, (Graduate Student Member, IEEE), AND
ALLEN L. GARNER^{1,2,3}, (Senior Member, IEEE)

¹School of Nuclear Engineering, Purdue University, West Lafayette, IN 47906, USA

²School of Electrical and Computer Engineering, Purdue University, West Lafayette, IN 47907, USA

³Department of Agricultural and Biological Engineering, Purdue University, West Lafayette, IN 47907, USA

Corresponding author: Allen L. Garner (algarner@purdue.edu)

This work was supported by the Office of Naval Research under Grant N00014-18-1-2341.

ABSTRACT Nonlinear transmission lines (NLTLs) have been increasingly studied to produce high power microwaves (HPM) at higher repetition rates than conventional HPM devices without requiring the same auxiliary systems. The ability to array NLTLs to produce higher power and achieve beam steering provides an additional capability. This review summarizes the various NLTL topologies designed to achieve these design objectives. Specifically, we summarize modeling and experimental studies for three primary topologies: the lumped element NLTL, the split ring resonator, and the traditional transmission line geometry using nonlinear materials. The lumped element NLTL and the traditional transmission line constructed with nonlinear materials lend themselves to higher power applications, while the split ring resonator is better suited for applications involving antennas. We provide a detailed summary of past studies for these topologies and conclude by exploring ongoing work and future opportunities for technological development.

INDEX TERMS Gyromagnetic, hybrid nonlinear transmission line, lumped element, nonlinear transmission line.


I. INTRODUCTION

The interest in nonlinear transmission lines (NLTLs) has increased in the past several decades because they can sharpen pulses to less than 100 ps [1] and serve as a solid state radiofrequency (RF) source. NLTL systems use components with nonlinear permittivity and/or permeability to sharpen pulses by allowing waves with higher amplitudes to travel faster than lower amplitude portions of the pulse to form an electromagnetic shock. Following electromagnetic shock-wave formation, oscillations occur due to the motion of either the dipole or magnetic moment of the nonlinear permittivity or permeability of the material, respectively. The shockwaves from a nonlinear dielectric transmission line induce oscillations with frequencies generally below 100s MHz. Nonlinear magnetic transmission lines can produce oscillations with frequencies up to low GHz after the material is saturated [1]. These oscillations occur either due to the precession of magnetic moments for nonlinear magnetic materials or the

translations of the dipole in the crystalline structure for nonlinear dielectric materials. The repetition rate, greater than 1 kHz, and consistency of the RF output make these devices practical for both low and high power RF applications [2], [3].

The technological development of fast, high voltage switching with capabilities up to hundreds of kHz [4]–[6] has motivated the development of high repetition rate RF sources with similar capabilities. Traditional microwave sources cannot operate at these high repetition rates because long electron recombination times increase the space charge in the gap, which limits microwave generation in traditional vacuum systems [7]. NLTLs provide a solid state RF source that can operate above 1 kHz with very little variation [3], [8].

While some systems provide high power capabilities by using high power components, such as lumped element designs [9], others provide a compact, narrowband, tunable design, such as split ring resonators (SRRs) [10]. Using nonlinear dielectrics in conventional transmission line configurations can achieve both high power and compactness [11]. Using these nonlinear materials in a coaxial design provides phase shifting, which allows beam combination and beam

The associate editor coordinating the review of this manuscript and approving it for publication was Davide Ramaccia .

steering to yield a directional, high power, high repetition rate RF source that can be tuned to meet various needs.

This review summarizes the different methods for constructing traditional NLTLs with either nonlinear permittivity or nonlinear permeability and the recent development of a hybrid NLTL with nonlinearity in both permittivity and permeability. We review the three main NLTL topologies (lumped element, split ring resonator (SRR), and nonlinear dielectric materials) both experimentally and theoretically. Section 2 summarizes lumped element NLTLs, Section 3 discusses SRRs, and Section 4 describes NLTLs designed using nonlinear dielectrics. We make concluding remarks in Section 5.

II. LUMPED ELEMENT NLTLs

Constructing NLTLs with lumped element circuits has allowed for more detailed studies of the physical phenomena and tunability of nonlinear effects by using circuit simulation software to analyze nonlinear capacitance and/or nonlinear inductance, as shown in Fig. 1. These circuits may be constructed using commercial off-the-shelf (COTS) devices and novel nonlinear components.

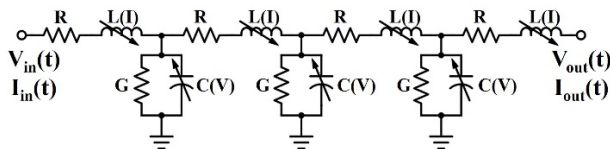


FIGURE 1. Lumped element representation of a nonlinear transmission line (NLTL) comprised of both nonlinear capacitance $C(V)$ as a function of voltage and inductance $L(I)$ as a function of current that translates an input voltage $V_{in}(t)$ and current $I_{in}(t)$ into an output voltage $V_{out}(t)$ and output current $I_{out}(t)$. An NLTL may be constructed with nonlinear capacitance and/or inductance. In general, loss may be included through a resistance R in series with the inductor or a conductance G in parallel with the capacitance.

The equation for the general, lossy, NLTL in Fig. 1 is given by

$$\frac{\partial^2 V(x)}{\partial x^2} = (j\omega L(I) + R)(j\omega C(V) + G)V(x), \quad (1)$$

where V is voltage, x is position along the line, ω is angular frequency, $L(I)$ is inductance as a function of current I , R is resistance in series with $L(I)$, $C(V)$ is capacitance as a function of V , and G is conductance in parallel with $C(V)$.

A. THEORETICAL CONTRIBUTIONS

Fundamental wave dynamics and transmission through nonlinear materials have been studied since the second half of the 20th century [12]. The mathematical solutions to the circuit equations often separate the incident pulse into solitons based on the amplitude to evaluate the wave speed of each soliton independently; these results demonstrate that higher amplitude solitons propagate faster than the lower amplitude ones [12]–[14]. These solutions can preserve the identities of the waves after their nonlinear interactions with each other, meaning that the solitons “pass through” one another and

reappear with virtually the same size or shape as prior to the interaction [12], [15]. The various solutions form arrays that can be optimized to achieve the shortest pulse rise time without oscillations when used as a pulse sharpening line [13]. For applications seeking RF oscillations, one may also determine the minimum NLTL length. Numerical techniques, such as the Bulirsch-Stoer or Runge-Kutta methods [12], [13], [16], have been used to solve the wave equation for the nonlinear circuits. The Runge-Kutta method is more efficient than the Bulirsch-Stoer method for very sharp rise times due to its simpler step calculation [13].

The circuit equations can also be simplified from a partial differential equation (PDE) to an ordinary differential equation (ODE) using Taylor series expansions and appropriate simplifications [14], [17]. This technique can model NLTLs with nonlinear capacitors made from metal oxide semiconductor (MOS) varactors. The simulations demonstrate the potential to sharpen both the rising and falling edges of the pulse [14]. As the wave propagates down the line, it is separated into various solitons; applying the output to a linear matched load, such as a resistor, reduces the oscillations because the various solitons interfere with one another [18]. Applying the output pulse to a much larger output resistance lowers signal amplitude losses, mitigating the oscillation issues [18]. Numerical simulations have also solved the resulting nonlinear PDEs derived through circuit analysis to determine the capacitance of nonlinear capacitors comprised of ionic polymer-metal composites [19].

NLTLs can be modeled with lumped elements by making the standard transmission line capacitance and inductance functions of voltage and current, respectively. The Korteweg-de Vries equation may be solved numerically for NLTLs comprised of nonlinear inductors with linear capacitors [20], nonlinear capacitors with linear inductors [9], and hybrid line configuration with nonlinear capacitors and nonlinear inductors [21], [22], discussed later in this review. The circuit model compared well with experimental results and showed how the frequency and output of the lines varied with nonlinearity. The output of nonlinear capacitive transmission lines used a decoupling capacitor to extract the AC signal, then applied to a load to allow for direct extraction [9].

Alternatively, one can separate the circuit analysis problem into different sub-problems by decoupling the linear and nonlinear subcircuits; balancing-related model reduction techniques reduce the linear subcircuit [23]. The reduction technique can be further refined by integrating the order-estimation algorithm with the proper-orthogonal decomposition reduction model to increase efficiency and decrease computational cost [24]. This can also be done for nonlinear inductors to solve for the magnetic vector potential and inductance as a function of current; results agree well with COMSOL simulations [25]. Another study used a multistage Adomain decomposition method, which is a hybrid analytical-numerical mathematical technique for solving nonlinear PDEs. This method is commonly used to model the transient behavior of nonlinear circuits, such as those

containing ferroelectric ceramic capacitors [26]. This approach solves a circuit model with a nonlinear resistor exhibiting cubic voltage-current dependence in series with a nonlinear capacitor exhibiting quintic voltage-charge dependence [26].

Characterizing the output from different NLTL topologies is critical for various applications in directed energy, pulsed power, and high power microwaves (HPM). SPICE circuit simulations of an NLTL can determine its output frequency and input pulse rise time sharpening [27]. Evaluating wave propagation through the NLTL elucidates the physics involved by characterizing complex wave interactions [28], which can be important for achieving desired performance. SPICE simulations have also verified theoretical modeling of wave propagation and RF generation in NLTLs [29].

More recently, researchers studied nonlinear Schottky diodes for NLTL applications. One group developed a model that evaluated the formation and propagation of a large-amplitude electromagnetic shock wave in an NLTL comprised of distributed Si and 4H-SiC diodes [30]. This group applied this model to extract n-layer thickness, breakdown voltage, total semiconductor thickness, optimum line length, minimum electrode thickness, normalized voltage drop along the electrodes, and normalized line width. This study further showed that the required rise time of the input pulse determined the maximum output voltage, concluding that SiC based diodes were better suited for high voltage applications compared to distributed Si [30]. The influence of imperfections in varactor diodes used as nonlinear capacitors in coupled NLTLs has also been studied. For NLTLs weakly capacitively coupled with a linear capacitance, a low impurity rate can cause leapfrogging due to potential acceleration of the soliton in the defect line [31].

B. EXPERIMENTAL CONTRIBUTIONS

While analytic models and simulations of lumped element NLTLs are valuable for system design, they must ultimately be compared to experimental results. Several studies have constructed NLTLs using COTS components such as nonlinear capacitors, nonlinear inductors, and hybrid lines. Experiments with COTS nonlinear capacitors agreed well with lumped element models [9]. Experimental results for hybrid NLTLs agreed well with the numerical models created using the Korteweg-de Vries method [22]. Another study applied a 30 ns pulse through a lumped element nonlinear inductor-based NLTL with saturable magnetic materials in an LC ladder network to generate an output RF frequency of 1 GHz at 20 MW peak power with a repetition rate of 1.0-1.5 kHz [32]. This study also constructed phased NLTL arrays to provide a higher power RF source [32].

Numerous materials have been used for NLTLs constructed with nonlinear capacitance COTS components. A parallel plate NLTL design used nonlinear capacitance from a lead-manganese-niobate ceramic (PMN38 from TRS company) and obtained the desired linear inductance by appropriately spacing capacitor sections [33]. The dielectric

loss was modeled as a series resistance based on the measured loss tangent of the NLTL. B-dot probes measured the pulses and current viewing resistors (CVRs) characterized the pulse evolution through the NLTL. An LTspice circuit model using the nonlinear capacitor model showed that the loss resistance prevented RF oscillations [33].

Evaluating COTS devices allows for better optimization and evaluation for their use in NLTLs. COTS capacitors constructed from lead-zirconate-titanate (PZT) and barium titanate (BT) were tested for their loss tangent, under different bias voltages, from 10 MHz to 1 GHz. The real and imaginary permittivities were extracted from the scattering parameters (S parameters) measured using a vector network analyzer (VNA). These studies showed that PZT capacitors were better suited for NLTLs because their capacitance changed more strongly as a function of applied voltage [34]. Another NLTL created using COTS capacitors with BT as the main component in the dielectric achieved measured rise-times between 1.84 and 2.5 μ s, in agreement with 2.2 μ s from simulations. The output pulse had a peak power of 8 kW for an output frequency of approximately 4 MHz [35].

Other studies evaluated COTS capacitors with X7R dielectric for use in NLTLs. Experiments showed that X7R NLTLs sharpened rise times down to tens of ns. Because the NLTL's cutoff frequency was 500 MHz, it could produce higher frequencies than other lumped element NLTLs with nonlinear capacitors. Simulations also showed that cross linking linear and nonlinear capacitors enabled frequency tuning [36]. A more recent approach for lumped element NLTLs leveraged the nonlinear capacitance of Schottky diodes to achieve a higher output frequency of 200 MHz, which agreed well with simulations. Continuing maturation of manufacturing techniques and improvement of material properties make Schottky diode NLTLs promising for higher frequency applications [37], [38]. Increasing the NLTL to a 30-section topology is expected to provide 65 W peak power and 115 V voltage modulation depth [38]. Double ridged guide antennas can extract and propagate the oscillations from the NLTL [39].

Using varactor diodes as nonlinear capacitors may produce up to 90% variation in their capacitance, although they are only useful at low voltages. However, an amplifier circuit utilizing MOSFETs can increase the voltage modulation depth from 10.7 V to 40 V for a frequency of 33.3 MHz [40]. The input pulse shape significantly effects the frequency generation and efficiency of the oscillations produced. One study showed that a 150 ns rectangular pulse was optimal compared to a half sine wave and triangular wave [41]. Because the rise time is a critical attribute of the input pulse, this study was somewhat misleading since the rectangular, triangular, and half sine pulses had different rise times.

Varactor diodes recently produced a left-handed NLTL that increased the third-harmonic signal fivefold compared to conventional left-handed NLTLs. The circuit topology generated edge states that produced higher harmonic signals at increased levels [42].

TABLE 1. Summary of lumped element NLTLs.

Study	Input Pulse Amplitude (V)	Input Pulse Duration (ns)	RF Generation Frequency (GHz)	RF Generation Output Peak Power	Nonlinear Component	Modeling Method
[14]	1.85	0.05	-	-	C	SONNET
[21]	6,000	600	0.05-0.08	5 kW	C&L	Korteweg-de Vries
[22]*	5	400	0.025-0.055	0.31 W	C	Korteweg-de Vries
[22]*	5	400	0.015-0.07	0.27 W	C&L	Korteweg-de Vries
[27]	10	150	0.04	-	C	SPICE
[32]*	30,000-50,000	60	1	20 MW	L	-
[33]	4,000-43,000	50	-	-	C	LT Spice
[35]	400	3270	0.004	8 kW	C	LT Spice
[36]	500	600	-	-	C	-
[37]	500	34	0.2	-	C	LT Spice
[127]	5	50	0.8	0.125 W	C&L	LT Spice
[128]	1,000	-	0.033	-	C&L	-

* tunable output frequency

C = Capacitor; L = Inductor.

Complementary metal–oxide–semiconductor (CMOS) technology provides a unique application for NLTLs as frequency multipliers. A frequency doubler and tripler were fabricated using CMOS processing to generate 20 GHz and 100 GHz, respectively. The 100 GHz tripler produced 0.7 W and a 12.2 dB bandwidth [43].

Table 1 summarizes the studies that evaluate lumped element NLTLs. While most lumped element NLTLs provide lower output power than NLTLs that utilize nonlinear materials, they elucidate the underlying physics in nonlinear wave propagation and can provide a more compact RF source.

III. SPLIT RING RESONATORS

SRRs comprised of different materials can provide nonlinear responses to input pulses, offering unique solutions to creating RF generators and narrowband signals. However, since SRRs are resonant structures resulting from the inductance produced by the ring structure and the capacitance from the gap g in Figure 2. The resulting oscillations will be narrowband without a nonlinear component. SRRs are generally small, with a correspondingly small power output; however, they may be arrayed to increase the total effective power. Figure 2 shows a representative coplanar, double SRR. This section describes modeling and experimental studies using SRRs and their application to NLTLs.

A. MODELING CONTRIBUTIONS

The initial work by Pendry and colleagues demonstrated that structures made of linear materials interacting with electromagnetic waves can exhibit negative permittivity and/or permeability [44], [45]. These studies showed that

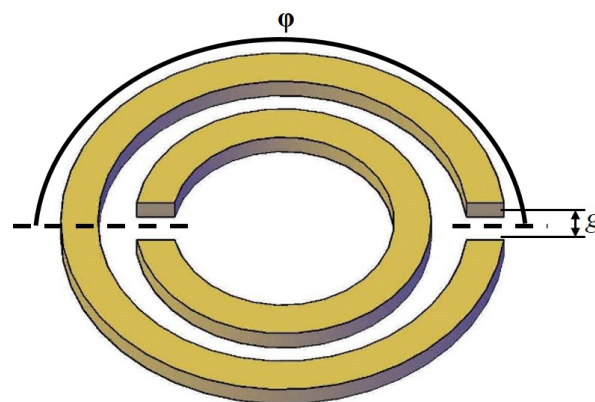


FIGURE 2. Coplanar split ring resonator circuit topology with gap width g and split angle ϕ .

microstructures built from nonmagnetic conducting sheets exhibit a tunable effective magnetic permeability, including the potential to induce large imaginary components. Internal capacitance and inductance made most of the structures resonant, enabling the enhancement of the nonlinearity [44].

SRRs can be combined in various geometries such as coplanar, where SRRs are coupled through interactions between their edges (EC-SRR), and coaxial, where SRRs are coupled through interactions between the broadsides of the structure. A quasi-analytical and self-consistent model was developed to determine the polarizabilities of SRRs. This model applied a local field approach to determine the dielectric parameters and resonance frequency of negative permeability and left-handed SRRs for both coplanar/edge coupled and coaxial/broadside coupled SRRs [46].

Another study evaluated three patterns of EC-SRR designs for placement onto a truncated pyramidal microwave absorber. CST Microwave Studio simulations for frequencies from 0.01-20 GHz showed that reflection loss decreased for all frequencies with the largest change from 15-20 GHz [47]. An outer split ring gap width (cf. Fig. 2) of $g = 0.02$ cm yielding the lowest reflection loss performance of the conditions studied [47].

Left hand (LH) wave propagation occurs when both permittivity and permeability are negative, thus reversing the vector orientation from a right handed orientation to a left handed orientation for the electric field \mathbf{E} , magnetic field \mathbf{H} , and the wave vector \mathbf{k} [49]. Coplanar waveguide (CPW) inductively coupled SRRs periodically loaded with narrow metallic wires yield the negative permeability required to achieve LH wave propagation in a narrow frequency band [48]. Prototypes exhibited high-frequency selectivity and low pass band insertion losses. Since the rings were smaller than the signal wavelength, the wavelength was easily tuned to the resonance frequency of 7.7 GHz [48]. Circular polarization selective surfaces have also been developed by placing planar SRRs coaxially and orienting the split to different positions, designated by φ in Fig. 2. A CST Microwave Studio model of this device showed resonant peaks at 9.75 and 10 GHz. The excellent agreement between simulation and experiments demonstrated the benefit for their application as an equivalent of gridded reflectors such as those used on satellites [50].

Narrow resonance bandwidth has motivated SRR research focused on increasing bandwidth. The bandwidth of an SRR may be increased by rotating its inner ring at different angles in a hybrid structure or changing its dimensions. Bandwidth increases of approximately 70% were proposed for such a unit cell comprised of three SRRs with different resonant frequencies, and SRR arrangement should be based on a descending and/or ascending resonant frequency order. Strip-line measurements confirmed that selecting either ascending or descending order did not change the loss tangent of the unit cell [51]. Models of these geometries have typically used analytic circuit models, which are limited to certain classes of structures and often fail to accurately predict the macroscopic behavior of metamaterials, or electromagnetic simulations, such as the finite integration method (FIM) or the finite element method (FEM) [52].

SRRs may be modeled with differential equations for current and voltage distributions and solved analytically to determine the resonant frequencies. An approximate solution for the lowest resonant frequency agrees with heuristic arguments and numerical simulations [53]. Alternatively, one may use simulation software, such as the MICRO-STRIPES package, a 3D electromagnetic simulation tool that solves problems in the time domain, or by replacing the distributed circuit with discrete circuits [53]. Treating the SRRs as inclusions in a bulk material allows development of a numerical model for double SRRs (cf. Fig. 2) to assess polarization for both planar and wire SRRs with the capacitance validated

using ANSOFT [54]. The resonant frequency of an SRR depends strongly on the capacitance of the structure. The resonant frequency for these devices depends on the gap surface capacitances, which may be determined using the equation for an electric field in a split cylinder combined with conformal mapping. These results showed that surface charges may play an important role in determining the total capacitance [55].

Coplanar SRRs can be developed into transmission lines [56] and antennas [57], [58], or stacked to create a metasolenoid [59]. A new approach for designing planar metamaterial structures was developed to investigate SRRs and complementary SRRs coupled to planar transmission lines. Baena, *et al.* derived analytic equivalent-circuit models of SRRs to show that stopband/passband characteristics of lines may be interpreted by negative/positive values of permittivity and permeability of the line in the long-wavelength limit [56]. Another study constructed a metamaterial SRR antenna with a very low profile and footprint that achieved an efficiency over 50% with a matched impedance of 50 Ω and a 120 MHz-10 dbm bandwidth [57]. The experimental performance of this system agreed well with Ansoft's HFSS full-wave simulations [57]. An SRR antenna designed using CST Microwave Studio provided two output frequencies: a higher frequency resulting from coupling a monopole radiator with the SRR at 4.59 GHz, and a lower frequency of the original monopole that resonated at 2.69 GHz [58]. HFSS simulations showed that a metasolenoid consisting of stacked SRRs may be modeled as a single particle and could achieve an effective permeability $\epsilon_{eff} > 10$ over a wide frequency range [59].

Treating the SRRs as inclusions or artificial magnetic inclusions in bulk materials can elucidate the bulk material's response to propagating electromagnetic waves. An effective medium theory showed the relationship between particle responses and a macroscopic system comprised of periodic resonant structures. This study used the average permittivity and permeability of each unit cell to derive a general form of discrete Maxwell equations for the macroscale material to determine the wave modes through the material; theoretically predicted S-parameters agreed well with HFSS simulations [60]. Quasi-static equivalent-circuit models for analyzing and designing multiple SRRs, spiral resonators, and labyrinth resonators extended recent models by considering a dielectric substrate with finite resistivity and losses due to the finite conductivity of SRR conductors. The models predicted the resonance and quality factor of the SRR, agreeing well with simulations and measurements [61]. Treating an SRR as an artificial magnetic inclusion showed the limitations of metamaterials based on geometry and physical characteristics. The flatness of permeability as a function of frequency is limited by the desired operational bandwidth of the structure. A circuit-based model yielded geometrically invariant fundamental constants, which showed that inclusions with large surface area induced higher permeability. Tradeoffs arose when attempting to simultaneously maximize

permeability and minimize loss/reducing dispersion for Swiss Rolls and SRRs [62].

Treating the SRR structure as a metacrystal with nonlinear magnetic properties also permits bulk material analysis. One study derived a perturbative solution to the nonlinear oscillator model of an SRR to characterize the nonlinear properties of the metacrystal. The metacrystal used exhibited a nonlinear magnetic response; the effective susceptibilities of the nonlinear magnetic response were evaluated by taking the series expansion to fifth order. The resulting expansion's validity was compared to valid power ranges observed experimentally. The modeled shift in resonant frequencies due to the increased power also agreed well with experimental results [63].

Using SRR structures in waveguides and with NLTLs reduces the noise in the output signal. Payandehjoo and Abhari discussed implementing compact complementary SRRs with a coplanar waveguide-based NLTL frequency doubler to suppress unwanted signals in NLTLs. They validated analytical derivations for the filter design and dispersion characteristics with VNA measurements. The third harmonic suppression was improved and sensitivity to variation of the input voltage level was reduced, producing a narrower signal. This filter increased isolation between the second and third harmonics at an input frequency of 500 MHz. These properties allowed for better single signal isolation. Components of the tank circuit of the distributed filter were determined using the Floquet Theorem; this method may also be applied to distributed amplifiers and mixers [64]. Other studies reported electromagnetic properties of waveguides loaded by complementary electric split ring resonators (CeSSRs) and the application of the waveguides in vacuum electronics. One study calculated the S-parameters of CeSSRs in free space using HFSS to retrieve the effective permittivity and permeability, the dispersion relation, and the gain of the wave-beam interaction. An effective medium theory (EMT) was used to calculate the modes of the waveguides as well as the gain. The HFSS results agreed well with EMT. This method improved agreement by fitting the permittivity tensor in the EMT; the gain of the backward wave mode of interaction with the electron beam calculated using HFSS and traveling wave tube theory agreed well with the dispersion method and EMT, respectively [65].

Recent studies have applied SRRs to HPM technology. One study considering metamaterials for HPM applications used an EMT to determine the coupling of an electron beam to a metamaterial structure in a geometry similar to a dielectric Cerenkov maser. The study analyzed negative real permeability, negative permittivity, and double-negative regimes of metamaterials. The authors analyzed SRRs and wire-rod materials by using the 3-D particle-in-cell (PIC) code ICEPIC to determine that the optimum coupling, and thus RF production, occurred in the negative permittivity regime [66]. Another study determined that the small size required for SRRs at higher frequency RF made them inadequate for high power applications due to electrical breakdown at high

electric field strengths. While the failure of a single element in an array (short or open circuit) reduced the array's output power, it did not change the resonant frequency. These structures provided a much more compact approach to HPM technology, but further work is required to make them feasible for high energy applications [67]. Some of the high electric fields produced in the SRRs arose due to field enhancement at the edges of the structure, making electrical breakdown a major design risk. One study investigated techniques for reducing the maximum field enhancement factors (MFEF) in different structures. One case study examined a Sievenpiper metasurface, a high impedance meta-surface that consists of periodically arrayed metal patch elements separated from the ground plane by a dielectric substrate and connected to ground by a thin pin through the substrate. A genetic algorithm evaluated negative and low-index metamaterials for field enhancement and presented a quad-beam focusing metamaterial lens with $MFEF < 5$ over the entire operating band for this metasurface. This approach was applied to negative-index metamaterial (NIM), zero-index metamaterial (ZIM), and low-index metamaterial (LIM) structures [68].

B. EXPERIMENTAL CONTRIBUTIONS

Materials comprised of SRRs provide unique engineering material properties. One composite media composed of SRRs achieved both negative permittivity and permeability and a transmitted bandwidth from 4.6 to 5.2 GHz [69]. The left-handed structure of this material also inverted the Doppler effect, Cherenkov radiation, and Snell's law [69]. Other studies have experimentally determined the material permittivity by examining signal interactions with the materials. One study examined the effective permittivity and permeability of composites containing wires and/or SRRs. This study demonstrated that wires/SRRs exhibited a frequency regime with negative permittivity/permeability, while combining the two structures yielded a negative component of the index of refraction in the frequency regime with negative permittivity and permeability [70].

The resonant frequency tunability of SRR systems makes them desirable for several applications, including antennas [51], tunable transmission lines [71], and waveguide filters [48]. One study varied the capacitance loaded between the split gaps in the SRR ring and the radial gap distance between the two rings to shift the resonant frequency. Reducing the capacitance increased the resonance and absorption of the SRR. A CST Microwave Studio simulation agreed well with the experimental results [72]. Another study created frequency tunable transmission lines using SRRs. Changing the gaps of the SRRs using PIN diodes, micro-electromechanical system (MEMS), and varactor diodes shifted the resonant frequency by 2.5 GHz [71].

SRR technology has the potential to increase transmission efficiency while decreasing electronics size. Placing an SRR in the near field of the aperture coupled strongly localized EM fields to a radius twenty times smaller than the resonance wavelength, increasing transmission by 740 times

TABLE 2. Summary of SRR technologies.

Study	Resonance Frequency (GHz)	Modeling Method	Gap Loading	Single/Double Ring	Coupling
[10]	5.407-5.84	-	Varactor	Double	Edge
[48]	7.7	CST	-	Double	Edge
[50]	9.75, 10	CST	-	Single	Axial
[53]	~1	MICRO-STRIPES	-	Double	-
[58]	2.69, 4.59	CST	-	Single	Edge
[63]	0.81-0.82/1.15-1.25 6.125-6.39,12.22-	CST	Varactor	Single/Double	Edge
[67]	12.55	HFSS	-	Double	Edge
[51]	0.6-0.775	HFSS	-	Double	Edge
[71]	6-9	Analytic Model	PIN Diode	Double	Edge
[73]	3.55-3.85	CST	-	Double	-
[75]	2.44-10.79	Not Stated	-	Double	Edge

by exciting the electric resonance of SRR at approximately 3.55-3.85 GHz [73]. Improved manufacturing techniques, such as fabrication in silver using nanosphere lithography, provide new possibilities for SRR technology. Scanning electron microscopy (SEM) showed that these SRRs had typical outer diameters between 100 and 140 nm, inner diameters between 40 and 60 nm, and gap widths between 35 and 40 nm. The measured results agreed well with calculations. The measured LC resonance wavelength was 721 nm, compared to the theoretically determined short wavelength limit of 426 nm [74].

NLTLs may be made from an array of SRRs with nonlinear capacitors placed in the gap. One study designed an NLTL system from varactor loaded SRRs to create a voltage controlled oscillator. Controlling the varactor diodes provided more frequency control frequency and creating a stripline [10], [63]. An ultra-wideband monopole antenna with a frequency range from 2.44 to 10.79 GHz was designed using two slotted SRRs. Simulations agreed well with measured data [75]; however, a low voltage breakdown threshold is a major design issue with SRRs, as discussed earlier. Both numerical and experimental studies have assessed the electric breakdown of SRRs under HPM exposure. In one experiment, an SRR combusted when exposed to 1 W at 10 GHz. EM simulation results at 10 GHz using the HFSS 3D full-wave EM field solver were imported into ANSYS to show that the peak temperature exceeded the combustion point of the FR4 PCB material used in the design [76].

SRRs provide a capability for creating metamaterials with unique material properties. While they do not offer a high power capability, they do offer frequency agility for propagating and filtering RF signals. Table 2 summarizes the capabilities of NLTL SRR technologies.

IV. NONLINEAR BULK MATERIALS

Ideally, NLTLs would simply be made from nonlinear materials; however, characterizing the physical behavior of these materials and designing effective manufacturing processes is challenging. Understanding the physics behind nonlinear material responses under various pulse parameters allows for optimizing designs for both pulse sharpening and RF output. Nonlinear bulk materials may be linear composites with nonlinear inclusions, a large piece of nonlinear electric or magnetic material, or a linear material that acquires nonlinear properties from its geometry such as SRRs. Each approach has been examined theoretically and experimentally to elucidate the behavior of these materials. Figure 3 shows a representative coaxial NLTL with a nonlinear material, which is typically a magnetic material with nonlinear permeability.

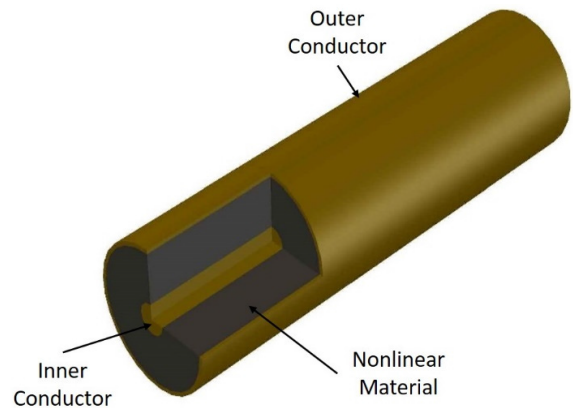


FIGURE 3. Coaxial nonlinear transmission line with a nonlinear material. Most coaxial or planar designs utilize nonlinear magnetic materials, although this material may also be a nonlinear dielectric or possess both nonlinear dielectric and magnetic properties.

Nonlinear materials are separated into ferroelectric, where the electric polarization may be reversed under an applied electric field, or the material ferromagnetic, where the material has an intrinsic dipole or magnetic moment. The intrinsic dipole in a ferroelectric material arises from the location of the atoms in the polycrystalline structure. Examples of ferroelectric materials include barium titanate (BT) and barium strontium titanate (BST). Applying an incident pulse to ferroelectric materials stresses the dipole, which will move around the crystalline structure to produce oscillations. The ferromagnetic materials may be biased, as in gyromagnetic lines, to align the magnetic moments normally in the axial direction. Applying a pulse generates a magnetic field that causes a precession of the magnetic moments to create an RF pulse. The microwave oscillations produced by ferroelectric materials produce lower frequency oscillations than ferromagnetic materials [77].

A. MODELING CONTRIBUTIONS

Nonlinear bulk materials have been studied for over fifty years [78]. Early studies analyzed the rotational model of flux reversal in ferromagnetic materials and their subsequent switching coefficients. This research led to the development of a rotational model based on flux reversal in ferromagnetic materials. Gyorgy theorized that normal materials have a minimum switching coefficient of $0.2 \mu\text{s}$ [78]. The switching coefficient evaluation can also be performed for NLTLs by investigating lossy NLTL systems. The Runge-Kutta method was used to characterize the coupling phenomenon, phase change, and power due to coupling two lossy transmission lines uniformly with uniform nonlinear shunt capacitances and series inductance [79].

The continuum-limit approximation and Gardner-Morikawa transformation were applied to the lumped element NLTL models from section 2.1 to derive a theory for a nonlinear magnetic lattice. The resulting modified Korteweg-de Vries equation from a four-terminal nonlinear LC network (equivalent circuit for nonlinear magnetic lattice) showed that the soliton, as a model of ferrimagnetic materials, is a solution of this equation; Hirota's method was then used to calculate the interaction of two solitons [80]. Ikezi, et. al. showed that creating a soliton pulse train in a nonlinear-dispersive system can create HPM bursts and proposed developing a modulated transmission line with a nonlinear dielectric [81]. They analyzed nonlinear wave evolution, found nonlinear dielectric parameter requirements to create this pulse, and demonstrated good agreement with some low-power experiments [81]. Other techniques, such as finite difference time domain (FDTD), may be used to calculate wave propagation. Applying FDTD to wave propagation through highly conductive nonlinear magnetic material exhibited good agreement with published numerical results using other approaches [82].

Many studies have investigated various materials to create nonlinear effects. Several NLTL studies have evaluated the effectiveness of ferroelectric materials on NLTLs. One such model that evaluated NLTLs [83] proposed invalid material

constraints since it was not bound by the laws of electrostatics and proposed invalid material constraints. However, other models [81] were physics-based and did not violate basic laws. Crowne developed a Mathematica code based on Kirchhoff's circuit laws that effectively modeled NLTL propagation [84].

These ferroelectric materials can also create nonlinear components for transmission line circuits. Nonlinear ferroelectric capacitors have also been evaluated for other circuit applications, such as creating an effective nonlinear inductance when used as loads for gyrator circuits [85]. Incorporating ZnO microvaristors, as inclusions in a rubber polymer, form composites with nonlinear conductive and dielectric properties. Properties were tuned by adjusting the inclusion concentration, and were predicted using percolation theory [85]. Other ferrites such as spinel, garnet, and hexaferrite have been used to create metamaterials [87]. Ferromagnetic microwires have also been used to create composites that may provide tunable electromagnetic properties by modifying the volume loading [88].

BST and BT are promising nonlinear materials. Crowne's Mathematica code for wave propagation in an NLTL showed promising results using BST [84]. Another numerical study assessed the pulse sharpening of BST and BT dielectric NLTLs, representing the material granularly using Voronoi polygons with a grain boundary model; calculating the capacitance determined material properties such as permittivity [89]. A theoretical model was developed to predict the permittivity of composites comprised of BT fibers with volume fractions between 0.0234 and 0.157. Theoretically predicted permittivity agreed well with measurements from 10 kHz to 10 MHz [90].

Although composite dielectric properties may be modeled in numerous ways [91]–[93], two main techniques have been applied for metamaterials. One is microscopic theory, where the parameters of each element are averaged to create a metamacroscopic property. This is used when the system properties are already known [94]. When the properties are unknown, the effective parameters must be determined using scattering parameters or transfer matrices. Numerical simulations may also be used upon determining the initial parameters for parts of the system. One numerical approach used a Green's function derived for nonlinear materials. Experimentally, nonlinear media have been created using SRRs in combination with nonlinear components. Using a nonlinear host material or substrate such as GaAs gave a higher output frequency. Small components with large field enhancement, such as SRRs and metal rods with high aspect ratio, significantly increased device nonlinearity [94].

One microscopic approach statistically modeled conductivity and inclusion aspect ratio distributions using the Maxwell Garnett mixing rule by treating the inclusions as conducting spheroids at a concentration below the 5% percolation threshold. Assuming a Gaussian distribution of 0.4 to 4% volume loading of carbon inclusions in Teflon, the authors used Maple 10 software to calculate complex

effective permittivity [95]. This study showed that the average aspect ratio and conductivity were the main factors influencing the composite effective permittivity at microwave frequencies [95]. Another study used HFSS to calculate scattering parameters to create an effective-medium model from the zero-scattering condition for calculating frequency-dependent effective permittivity and permeability of metamaterials. The model used a dipole approximation with no additional long-wavelength approximations. It also captured the effects of spatial dispersion and predicted finite effective refractive index and antiresonances in agreement with finite-element calculations [96]. The resulting high frequency mixing rule agreed well with the Maxwell Garnett mixing rule and yielded scattering parameters for composites similar to metamaterials of SRRs or particles arranged in a fishnet structure [97].

Multiple studies have recently examined wave motion through nonlinear materials in an NLTL configuration. One study modeled wave propagation in an NLTL using the derivative nonlinear Schrödinger equation with constant potential in the small amplitude, long wavelength limit, noting that some exact elliptic solutions showed mirror or rotational symmetry [98]. Another study investigated stationary solutions in the form of traveling EM waves in a uniform transmission line with saturated ferrites and no damping. This model showed that the period of linear oscillations increased linearly with current, while the group velocity of stationary waves increased with oscillation amplitude. Increasing the external magnetic field increased the asynchronicity of the oscillation [99]. An analytical model supported by SPICE circuit simulations was derived to study the wave propagation through a gyromagnetic line, specifically pulse rise time compression, by changing NLTL parameters. Several models were used with various parameters: Weiner and Silber's model, a simplified theory on pulse sharpening, had an input of 6 kV and 40 ns rise and fall times; Pouladian-Kari *et al.*'s model, which calculated the reduction of the output rise time due to the decrease in permeability, had an input of 12 kV and a 3.5 ns rise time; and Dolan and Bolton's model had an input of -10 kV with a rise time of 2 ns and produced 5 GHz oscillations. The numerical analysis was done using Mathematica [100].

Wave sharpening, oscillation generation, and wave propagation can be modeled very accurately by using FDTD to solve the Landau-Lifschitz-Gilbert equations, given by [101]

$$\frac{\partial \mathbf{M}}{\partial t} = -\gamma \mu_0 \mathbf{M} \times \mathbf{H} + \frac{\alpha \mu_0}{M_s} \left[\mathbf{M} \times \frac{\partial \mathbf{M}}{\partial t} \right], \quad (2)$$

where \mathbf{H} and \mathbf{M} are the magnetization and total magnetic field vectors, respectively, μ_0 is the permeability of free-space, M_s is the value of the saturated magnetization, γ is the electron gyromagnetic ratio, and α is a dimensionless damping parameter. A model simulating the conversion of a DC pulse into a quasi-monochromatic RF pulse agreed well with the synchronous wave model. The study showed that the central frequency of the wideband pulse produced by the

NLTL did not depend solely on the precession of the magnetic moments. The total coaxial NLTL diameter, ferrite core size, line spatial filling, and center frequency electric and magnetic parameters were also affected by the eigenmodes in the line and their associated frequencies and dispersion [102].

B. EXPERIMENTAL CONTRIBUTIONS

Nonlinear dielectrics have been incorporated into transmission lines for over thirty years [2], [34], [81]. Using various dielectrics and geometries gave a broad range of shock forming lines [103], NLTLs for pulse sharpening, or RF sources. Ferrite loaded coaxial lines were used to produce sub-ns high voltage pulses through magnetic compression [103]. Early research examined issues with various geometries for NLTL design. Since coaxial geometry generates nonuniform fields, some researchers decided to use a parallel plate geometry for a shock forming line. The authors also found that BST could achieve a very high relative permittivity (~8000-13 000), making it ideal for NLTLs. Experiments with BST achieved a shock wave amplitude of approximately 13 kV with a rise-time of 7 ns. At the load, 20-30% of the shock wave amplitude was reached in 20 ns with rise times of 700 ps or less (measurement sensitivity limited rise time determination for faster rise-times) [104].

While this review mainly focuses on using NLTLs as solid state RF generators, one useful application of NLTLs is for pulse compression [105]. Recently, a two-stage magnetic compressor based on gyromagnetic NLTLs converted a 7 ns duration, 500 kV amplitude input pulse into a 30 GW peak power output pulse with 0.65 ns duration, 1.1 MV amplitude, and a 1 kHz repetition rate [106]. Another system used a single, 30 cm long NLTL with an axially biased magnetic field of 22 kA/m to sharpen a 70 kV input pulse to a final rise time of 350 ps with an amplitude > 90 kV at a 1 kHz repetition rate [107]. More recently, nonlinear ferrite lines sharpened a 4 ns full-width half-maximum (FWHM) -500 kV pulse to a 45 ps, 850 kV pulse with an increase rate of the leading pulse of 15.5 MV/ns [108]. An axial bias field was added to produce microwave frequency of 3-3.7 GHz pulses with a 65%-85% modulation depth, although the repetition rate was limited to 1 Hz due to high electric fields in the line [108].

Researchers have used other nonlinear materials to create NLTL RF sources. One study used saturated NiZn ferrite to construct an NLTL with output oscillations at 1 GHz for bursts of 1000 pulses at 200 Hz repetition rate. A 1 m coaxial line sharpened a 250 kV pulse from a 2.5 ns rise time to 0.5 ns rise time, with RF pulse duration of 4-5 ns and a peak power of 260 MW [11].

More recently, NLTLs have been used to construct solid state RF sources with high repetition rates using solid state switching technology. A 50 kV 4H-SiC photo-conducting solid state switch triggered with a 3 mJ Nd:YAG laser switched a capacitive discharge circuit into an NLTL, comprised of ferromagnetic pieces in a coaxial geometry. The resulting pulse had a FWHM of 7 ns with a 2 ns rise time

and repetition rate up to 65 MHz. This generated 2.1 GHz microwaves with 50 Ω system impedance [109]. This line achieved peak powers over 30 MW with a 30 kV incident pulse. The RF power output reached 4.8 MW peak, with an RF pulse length ranging from 1-5 ns. The NLTL operated in S-band, with about 30% bandwidth. Varying the nonlinear material's bias magnetic field established active delay control. Tuning the NLTL's magnetic bias varied the system's electrical delay between 9 ns and 20.5 ns [110]. Adjusting another NLTL's bias field tuned its frequency from 0.95 to 1.45 GHz. Circuit models and frequency domain simulations supported these experiments. A Marx generator provided 25 ns pulses with a 5 ns rise time, voltages up to 260 kV, peak power levels above 100 MW, average power levels of tens of MW, and 4-17 ns RF pulse duration. The output transition line provided 14 ns of transit time isolation from potential interference from the reflected pulse from the load [111].

NLTL RF outputs can be combined and controlled in various ways. One RF source used a gyromagnetic NLTL comprised of NiZn ferrites to generate MW-level power for L, S, and C microwave bands. A bias field controlled delay power combiner was designed for these bands. COMSOL was used to model the combiner to determine its functionality and power limits. The combiner joined two 50 Ω coaxial inputs to a single tapered transition with a final output impedance of 50 Ω . The NLTL output frequency was between 1.8 and 2.6 GHz [112]. Another study aligned a coaxial, four-element NLTL antenna array by placing adjustable, temporal ferromagnetic delay lines serially in front of the main NiZn ferrite loaded gyromagnetic NLTL. Delay line propagation velocity adjustability was achieved by varying its bias voltage or external DC magnetic field [113]. Connecting one high voltage driver to two gyromagnetic NLTLs provided electronically controlled beam steering. Each NLTL produced several ns RF pulses with peak power from 50 to 700 MW and generated frequencies from 0.5 to 1.7 GHz at a repetition rate of 100 Hz. A helix antenna radiated RF pulses with near-circular polarization at 350 MW peak power level. The input pulse rise times were approximately 2-3 ns [114]. Since some NLTLs cannot produce high output power, combining the output of multiple NLTLs has been of great interest. We previously described a solid state, four-element array gyromagnetic NLTL comprised of NiZn ferrites with frequency adjustable between 2-4 GHz using a magnetic field with a repetition rate of 1 kHz and a power of 4.2 MW. This four NLTL system used phase control to create an additive effect on the RF output that lasted \sim 2 ns [115].

Other parallel gyromagnetic NLTL phase adding was accomplished by using a solenoid to create a magnetic field. A 430 kV, 5 ns input pulse produced oscillations that reached 175 kV at the NLTL output, with a frequency of \sim 4 GHz and an electric field of 250 kV/m at 3 m distance, at a repetition rate of 1 kHz. The NLTLs were made of NiZn rings, yielding an RF output 2-4 ns in duration [116]. More recently, Ulmaskulov *et al.* demonstrated NLTL summation by combining four ferrite based NLTLs that produced 8 GHz

pulses with an input nanosecond pulse of -195 kV, at a repetition rate of 5 Hz, for a total duration of 20 s [117]. Others coupled NLTLs, combining the output using an external bias. The application of high voltage nanosecond pulses generated 1 s packets of 1000 Hz RF from the output of the four channels. The RF signal had a pulse amplitude of 175 kV, generating an effective frequency of approximately 4 GHz for the NiZn ferrite NLTL [8]. Four coherent gyromagnetic NLTLs produced 2.1 GHz pulses with an effective potential of 360 kV at the radiation axis, at a repetition rate of 1 kHz. A variation of 17° through beam steering was demonstrated in the horizontal plane [118].

Other nonlinear materials have been explored. The permittivity and permeability of barium titanate-ferrite was examined for application in a nonlinear capacitor exhibiting nonlinearity under high voltage pulses. The metamaterial and insulation of magnetic particles with a dielectric layer were tested [119]. Another study constructed a stripline gyromagnetic NLTL from yttrium iron garnet ferrite. The RF source operated at 40.1% average bandwidth and 2-12.7 MW peak power [120]. $\text{Na}_{1/2}\text{Bi}_{1/2}\text{Cu}_3\text{Ti}_4\text{O}_{12}$ ceramics were examined for dielectric tunability. The resulting Schottky and Langevin effects achieved \sim 70% tunability at room temperature for a 200 V/cm field. The positive tunability could be switched to negative tunability by 10% overdosing of Bi [121]. Another metamaterial, nanocomposite $\text{Ag}/\text{Zr}_{0.9}\text{Ni}_{0.1}\text{O}_y$, was interrogated with a quadrupole electrode AC electric field. The Ag nanoparticles aligned parallel to the electric field. The surface was evaluated using x-ray diffraction, SEM, and transmission electron microscopy. A frequency scan of a nanocomposite capacitor measured permittivity, while permeability was determined by wrapping a wire around the composite and measuring the wire's inductance during a frequency scan from 0 to 10 GHz; these measurements showed potential for the nanocomposite to be a double negative material [122].

The maturation of NLTL technology has raised other potential applications of the technology. One study examined the effects of RF pulses with a ns envelope on biological samples. The RF pulse amplitude was varied by 52 dB with about 40 kV/cm maximum output field, 4-25 ns pulse duration, and 0.6-1.0 GHz frequency [123]. Other researchers operated a gyromagnetic NLTL as a peak power amplifier of an input pulse, with similar pulse duration, and most of the input energy transmitted to the first oscillation peak. Experiments applied a 500 kV, 7 ns half height pulse duration pulse with about 300 MHz frequency input to the NLTL, yielding a 740 kV, 2 ns duration output, and 6 to 13 GW amplification [124]. Using the NLTL in a high current environment permitted its use in a gigawatt class electron beam driver. Experiments showed 0.95-1.45 GHz peak frequencies and 5-35% amplitude modulations depending on the setup [125]. This GW-class electron beam was simulated using PIC and measured waveforms from a synchronous wave ferrite NLTL to demonstrate its practicality. Simulations coupling the modulated beam to a disk-on-rod slow wave structure (SWS)

TABLE 3. Summary of NLTLs designed with nonlinear materials.

Study	Input Pulse Amplitude (kV)	Input Pulse Duration (ns)	Repetition Rate (kHz)	RF Generation Frequency (GHz)	RF Generation Output Peak Power (MW)
[8]	-175	5	1	4	-
[11]	250	10	0.2	1	260
[108]	20-25	7	65,000	2.1	-
[109]	30	1-5	-	2-4	4.8
[110]	260	25	-	0.95-1.45	100
[113]*	240	2-3	0.1	0.5-1.7	50-700
[114]*	-40	-	1	2-4	4.2
[115]*	-430	5	1	4	166
[116]*	-195	1	0.005	8	-
[117]*	-200	5	1	2.1	344
[119]	35-55	-	-	0.62-0.96	2-12.7
[120]	150-190	-	-	0.8-1.8	50-200

* combined output

increased extractable RF ten times compared to direct extraction from an NLTL [126].

Recent studies utilized different ferrites and insulating materials for spatially dispersive NLTLs. One study replaced transformer oil with SF₆, which increased the RF output power by approximately a factor of four at frequencies exceeding 1.2 GHz; however, the peak power decreased at the center frequency. The output frequency range of the NLTL increased from 800 MHz - 1.4 GHz for transformer oil to 900 MHz- 1.8 GHz for SF₆. The highest power output for the transformer oil NLTL with an input pulse of 34 kV was ~ 230 MW at ~ 1 GHz, while the peak output power using SF₆ for the same input pulse was ~200 MW at 1.4 GHz. Also, using nickel zinc ferrites with higher permeability (800 vs. 16) and lower resistivity (10⁵Ω·cm vs. 10⁸Ω·cm) increased peak power generation [127].

NLTLs utilizing nonlinear dielectric or nonlinear magnetic materials provide a solid state HPM option. Phasing multiple NLTLs increases power and steerability without mechanical components. The lack of auxiliary systems, such as vacuum pumps, greatly reduces the physical footprint of these systems and increases power density. Output frequency is determined by the nonlinear material used; NLTLs using nonlinear dielectric materials yield less than 100 MHz, while NLTLs using nonlinear magnetic materials produce up to 8 GHz. Researchers are on the verge of producing GW class systems that can rival traditional vacuum HPM systems. A summary of NLTLs with nonlinear materials is given in Table 3.

V. HYBRID NLTLs

The above research generally studied NLTLs that achieved their nonlinearity using either a nonlinear permittivity or a nonlinear permeability; however, recent research has

investigated hybrid NLTLs that exhibit both nonlinear permittivity and permeability. Hybrid NLTLs were created using a SPICE simulation and experiments to create a chaos generator, which could be potentially valuable for modeling naturally occurring phenomena. The nonlinear circuit equations were solved using the Runge-Kutta method [16]. SPICE was used to simulate the frequency generation above 800 MHz using a hybrid line using varactor diodes as nonlinear capacitive elements. The system had 10 V applied voltage, 50 Ω impedance, and input pulse parameters of 5 V amplitude, 40 ns rise time, and 50 ns FWHM pulse width. The rise time decreased to 18-22 ns using proprietary ferrites; simulations showed about 800 MHz output frequency, with proposed 1-2 GHz using proprietary ferrites (BAE Systems, UK). The authors also demonstrated how utilizing a hybrid NLTL produced a longer, 15 ns RF envelope compared to ~7 ns RF envelope for NLTLs with only nonlinear capacitance [115], [128].

A numerical model for a lumped element hybrid NLTL used the Korteweg-de Vries equation. This analysis agreed well with experiments, which used COTS nonlinear inductors and nonlinear capacitors that varied exponentially with current and voltage, respectively. The output frequency of the modeled hybrid line was 50% greater than similar NLTLs with only nonlinear capacitance or nonlinear inductance. Modeling the hybrid NLTL showed that the frequency doubled over a 5V increase in the voltage bias. [22]. A hybrid NLTL constructed of COTS components was tested with a rectangular input pulse with a 6 kV input voltage, 600 ns pulse width, 47 ns rise-time, and 44 ns fall-time, using a storage capacitor and a fast semiconductor switch. Component nonlinearity was evaluated to determine line impedance change to match the load and prevent reflections. The RF produced

TABLE 4. Comparison of key NLTL parameters for various designs.

	Lumped Element NLIL	Lumped Element NLCL	SRR	Nonlinear Material	Hybrid NLTL
Frequency (GHz)	0.7-1.3	0.01-0.2	2.44-12.5	0.95-8	0.8-2
RF Pulse Width (ns)	400	300	-	1-25	500
Peak Power (MW)	20	0.008	5×10^{-9}	4.8-700	0.005
Maximum Input Voltage (kV)	43	50	0.001	430	6
Nonlinear Element	L	C	C	L	L&C

NLIL = Nonlinear Inductive Line; NLCL = Nonlinear Capacitor Line; SRR = Split ring resonator

by the line varied between 55 MHz and 80 MHz for 5 kV and 8 kV pulse voltages, respectively. The power output of the line peaked at around 5 kW for a 40 Ω load. Simulations using a code developed by the researchers matched well with the experimental results [21].

A more recent study constructed two 30-section hybrid NLTLs with BT dielectrics nonlinear capacitors, 2.2 nF or 10 nF unbiased capacitance, and ferrite bead inductors. A 1 kV input pulse applied to the lines generated a 33 MHz output. The voltage modulation depth of the output signal was 700 V for the NLTL with the 2.2 nF capacitors and 200 V for the 10 nF capacitors. Ten RF cycles were produced for each input pulse applied to the lines. The authors showed that the hybrid NLTLs produced a higher voltage modulation depth compared to lines with a single nonlinear component [116], [129].

Other studies evaluated hybrid NLTLs as soliton generators, developing a model based on a modified Korteweg De-Vries equation and SPICE simulations.

Compared to traditional NLTLs using only nonlinear capacitors, hybrid lines produced more oscillations, although at lower voltages. For instance, the traditional NLTL produced a single peak with 8 V amplitude, while the hybrid NLTL produced three solitons with the highest peak at 4 V and the lowest peak slightly less than 2 V. The numerical model developed by the authors matched well with SPICE simulations [117], [130].

VI. CONCLUSION

NLTLs have a promising future as valuable solid state RF sources. NLTLs may be designed using different modalities with unique advantages and disadvantages. Table 4 compares key parameters of the NLTL topologies.

The lumped element approach allows for a more modular configuration that may be used at higher voltages due to circuit design and higher voltage components. However, the lumped element approach can become physically large when adding more stages at higher voltages and the NLTL output is not as tunable as other designs. The Bragg cutoff frequency limits the output frequency of lumped element designs to less than 250 MHz for diode based systems, and even lower for capacitor based systems. The SRR approach provides a narrowband structure that can be used as an NLTL

by adding nonlinear components or a nonlinear substrate. The frequency can be changed by illuminating the gaps during operation; however, this may be impractical for a mobile system. The SRR approach is limited in power due to the small structure size required for the desired RF output frequencies. SRRs are more practical as waveguide filters or steerable antennas, although they could provide compact low power RF generators. NLTL designs with nonlinear materials enhance device compactness and provide some frequency flexibility by changing the NLTL's bias. This approach also allows for creating phased arrays for potential power combination and beam steering. However, unless combined with other devices such as an SWS, the nonlinear material approach limits the power output compared with the lumped element method [111]. The RF envelope of these devices has been an issue; most RF pulses were on the order of a few ns, although hybrid NLTLs may potentially extend this operating range [128]. Hybrid NLTLs also provide a unique capability for matching modulators to antennae in system designs through controlling both nonlinear permittivity and nonlinear permeability to achieve a more constant impedance. Table 5 shows the best NLTL topology for optimizing frequency, RF pulse width, peak power, ease of construction, and load matching.

TABLE 5. Optimal NLTL topology for a given parameter.

	Lumped Element	SRR	Nonlinear Material	Hybrid NLTL
Frequency		X		
RF Pulse Width				X
Peak Power			X	
Ease of Construction	X			
Load Matching				X

Nonlinear material based NLTLs are optimal for high power RF generation because of phase coupling. SRRs are optimal for a low power, high frequency RF generator or antenna where combining the output produces directivity. Lumped element NLTLs are best suited for mid-range power applications due to component limitations. The ability to

utilize nonlinear inductance and capacitance in the lumped element topology allows for more design customization.

Current research focuses on overcoming the challenges when incorporating NLTLs into a system with limited power availability and combining NLTLs with a matched antenna to mitigate loss and reflections. Researchers are exploring the addition of coaxial ceramic rings to gyromagnetic NLTLs to improve their efficiencies, typically around 10%. Adding rings with a permittivity of 50 increased the overall line permittivity from 3.8 to 5.9, which increased the output from 35 kV to 50 kV and shifted the output frequency from 1.25 GHz to 1.17 GHz [131]; further optimization could increase the NLTL efficiency from 10% to over 40%. Researchers have also investigated RF power extraction from an NLTL by using a resistive load to optimize the output. Theoretical models and SPICE simulations of efficiency agreed well with experimental results [132]. This work will be crucial for extending NLTL designs to LC loads more comparable to some antenna designs.

In summary, we have reviewed the three main topologies for NLTLs. Lumped element and nonlinear material designs are promising for HPM applications, while SRR designs are more applicable for lower power systems and antenna applications. NLTLs are a promising technology for providing high power (>100 MW), high frequency (>1 GHz), and high repetition rate (>1 kHz) solutions in a solid state package, while greatly decreasing the need for auxiliary systems required compared to traditional HPM technology. Current research demonstrates the feasibility of increasing the frequency of nonlinear capacitor-based lines simultaneously with increasing power output and efficiency. Ongoing advancements in solid state switch technology will make the application and optimization of NLTLs more important in future HPM system development.

ACKNOWLEDGMENT

The authors thank Naval Surface Warfare Center Dahlgren Division for assistance in obtaining additional resources and references.

REFERENCES

- [1] J.-W.-B. Bragg, J. C. Dickens, and A. A. Neuber, "Ferrimagnetic nonlinear transmission lines as high-power microwave sources," *IEEE Trans. Plasma Sci.*, vol. 41, no. 1, pp. 232–237, Jan. 2013.
- [2] J. O. Rossi, L. P. Silva, J. J. Barroso, F. S. Yamasaki, and E. Schamiloglu, "Overview of RF generation using nonlinear transmission lines," in *Proc. IEEE Pulsed Power Conf. (PPC)*, May 2015, pp. 1–6.
- [3] J. Gaudet, E. Schamiloglu, J. O. Rossi, C. J. Buchenauer, and C. Frost, "Nonlinear transmission lines for high power microwave applications—A survey," in *Proc. IEEE Int. Power Modul. High Volt. Conf. (PMHVC)*, May 2008, pp. 131–138.
- [4] O. S. F. Zucker, P. K. L. Yu, and Y.-M. Sheu, "GaN switches in pulsed power: A comparative study," *IEEE Trans. Plasma Sci.*, vol. 42, no. 5, pp. 1295–1303, May 2014.
- [5] T. J. Flack, B. N. Pushpakaran, and S. B. Bayne, "GaN technology for power electronic applications: A review," *J. Electron. Mater.*, vol. 45, no. 6, pp. 2673–2682, Jun. 2016.
- [6] X. She, A. Q. Huang, Ó. Lucía, and B. Ozpineci, "Review of silicon carbide power devices and their applications," *IEEE Trans. Ind. Electron.*, vol. 64, no. 10, pp. 8193–8205, Oct. 2017.
- [7] S. Ashby, R. R. Smith, N. Aiello, J. N. Benford, N. Cooksey, D. V. Drury, B. D. Harteneck, J. S. Levine, P. Sincerny, L. Thompson, and L. Schlitt, "High peak and average power with an L-band relativistic magnetron on CLIA," *IEEE Trans. Plasma Sci.*, vol. 20, no. 3, pp. 344–350, Jun. 1992.
- [8] M. R. Ulmasculov, K. A. Sharypov, S. A. Shunailov, V. G. Shpak, M. I. Yalandin, M. S. Pedos, and S. N. Rukin, "Gyromagnetic nonlinear transmission line generator of high voltage pulses modulated at 4 GHz frequency with 1000 Hz pulse repetition rate," *J. Phys. Conf. Ser.*, vol. 830, May 2017, Art. no. 012027.
- [9] N. S. Kuek, A. C. Liew, E. Schamiloglu, and J. O. Rossi, "Pulsed RF oscillations on a nonlinear capacitive transmission line," *IEEE Trans. Dielectr. Electr. Insul.*, vol. 20, no. 4, pp. 1129–1135, Aug. 2013.
- [10] J. Choi and C. Seo, "Broadband VCO using electronically controlled metamaterial transmission line based on varactor-loaded split-ring resonator," *Microw. Opt. Technol. Lett.*, vol. 50, no. 4, pp. 1078–1082, Apr. 2008.
- [11] I. V. Romanchenko, V. V. Rostov, V. P. Gubanov, A. S. Stepchenko, A. V. Gunin, and I. K. Kurkan, "Repetitive sub-gigawatt RF source based on gyromagnetic nonlinear transmission line," *Rev. Sci. Instrum.*, vol. 83, no. 7, Jul. 2012, Art. no. 074705.
- [12] R. Hirota and K. Suzuki, "Theoretical and experimental studies of lattice solitons in nonlinear lumped networks," *Proc. IEEE*, vol. 61, no. 10, pp. 1483–1491, Oct. 1973.
- [13] M. M. Turner, G. Branch, and P. W. Smith, "Methods of theoretical analysis and computer modeling of the shaping of electrical pulses by nonlinear transmission lines and lumped-element delay lines," *IEEE Trans. Electron Devices*, vol. 38, no. 4, pp. 810–816, Apr. 1991.
- [14] E. Afshari and A. Hajimiri, "Nonlinear transmission lines for pulse shaping in silicon," *IEEE J. Solid-State Circuits*, vol. 40, no. 3, pp. 744–752, Mar. 2005.
- [15] N. J. Zabusky and M. D. Kruskal, "Interaction of 'solitons' in a collisionless plasma and the recurrence of initial states," *Phys. Rev. Lett.*, vol. 15, no. 6, pp. 240–243, Aug. 1965.
- [16] M. Tokuyama and H. Ohtagaki, "Chaos in a series circuit with a nonlinear capacitor and a nonlinear inductor," *Electr. Eng. Jpn.*, vol. 150, no. 2, pp. 35–42, Jan. 2005.
- [17] E. Afshari, H. S. Bhat, A. Hajimiri, and J. E. Marsden, "Extremely wideband signal shaping using one- and two-dimensional nonuniform nonlinear transmission lines," *J. Appl. Phys.*, vol. 99, no. 5, Mar. 2006, Art. no. 054901.
- [18] J. D. C. Darling and P. W. Smith, "High-power pulsed RF extraction from nonlinear lumped element transmission lines," *IEEE Trans. Plasma Sci.*, vol. 36, no. 5, pp. 2598–2603, Oct. 2008.
- [19] Z. Chen, D. R. Hedgepeth, and X. Tan, "Nonlinear capacitance of ionic polymer-metal composites," *Proc. SPIE*, vol. 7287, no. 517, 2009, Art. no. 728715.
- [20] N. S. Kuek, A. C. Liew, E. Schamiloglu, and J. O. Rossi, "Oscillating pulse generator based on a nonlinear inductive line," *IEEE Trans. Plasma Sci.*, vol. 41, no. 10, pp. 2619–2624, Oct. 2013.
- [21] N. S. Kuek, A. C. Liew, E. Schamiloglu, and J. O. Rossi, "RF pulse generator based on a nonlinear hybrid line," *IEEE Trans. Plasma Sci.*, vol. 42, no. 10, pp. 3268–3273, Oct. 2014.
- [22] N. S. Kuek, A. C. Liew, E. Schamiloglu, and J. O. Rossi, "Circuit modeling of nonlinear lumped element transmission lines including hybrid lines," *IEEE Trans. Plasma Sci.*, vol. 40, no. 10, pp. 2523–2534, Oct. 2012.
- [23] A. Steinbrecher and T. Stykel, "Model order reduction of nonlinear circuit equations," *Int. J. Circuit Theory Appl.*, vol. 41, no. 12, pp. 1226–1247, Dec. 2013.
- [24] B. Nouri, M. S. Nakhla, and R. Achar, "Efficient simulation of nonlinear transmission lines via model-order reduction," *IEEE Trans. Microw. Theory Techn.*, vol. 65, no. 3, pp. 673–683, Mar. 2017.
- [25] E. Stenglein and M. Albach, "Analytical calculation method for the non-linear characteristic of ferrite-cored inductors with stepped air gap," *Electr. Eng.*, vol. 99, no. 1, pp. 421–429, Mar. 2017.
- [26] H. Fatoorehchi, H. Abolghasemi, and R. Zarghami, "Analytical approximate solutions for a general nonlinear resistor-nonlinear capacitor circuit model," *Appl. Math. Model.*, vol. 39, no. 19, pp. 6021–6031, Oct. 2015.
- [27] F. S. Yamasaki, L. P. S. Neto, J. O. Rossi, and J. J. Barroso, "Soliton generation using nonlinear transmission lines," *IEEE Trans. Plasma Sci.*, vol. 42, no. 11, pp. 3471–3477, Nov. 2014.
- [28] S. Y. Elnaggar and G. N. Milford, "Description and stability analysis of nonlinear transmission line type metamaterials using nonlinear dynamics theory," *J. Appl. Phys.*, vol. 121, no. 12, Mar. 2017, Art. no. 124902.

- [29] M. S. Nikoo, S. M.-A. Hashemi, and F. Farzaneh, "Theory of RF pulse generation through nonlinear transmission lines," *IEEE Trans. Microw. Theory Techn.*, vol. 66, no. 7, pp. 3234–3244, Jul. 2018.
- [30] A. S. Kyuregyan, "Large-amplitude shock electromagnetic wave in a nonlinear transmission line based on a distributed semiconductor diode," *Semiconductors*, vol. 53, no. 4, pp. 511–518, Apr. 2019.
- [31] N. A. Akem, A. M. Dikandé, and B. Z. Essimbi, "Leapfrogging of electrical solitons in coupled nonlinear transmission lines: Effect of an imperfect varactor," *Social Netw. Appl. Sci.*, vol. 2, no. 1, Jan. 2020.
- [32] N. Seddon, C. R. Spikings, and J. E. Dolan, "RF pulse formation in nonlinear transmission lines," in *Proc. 16th IEEE Int. Pulsed Power Conf.*, Jun. 2007, pp. 678–681.
- [33] D. M. French, B. W. Hoff, S. Heidger, and D. Shiffler, "Dielectric nonlinear transmission line," in *Proc. IEEE Pulsed Power Conf.*, Jun. 2011, pp. 341–345.
- [34] L. P. S. Neto, J. O. Rossi, J. J. Barroso, and A. R. Silva, "Characterization of ceramic dielectrics for sub-GHz applications in nonlinear transmission lines," *IEEE Trans. Plasma Sci.*, vol. 42, no. 10, pp. 3274–3282, Oct. 2014.
- [35] L. P. Silva Neto, J. O. Rossi, J. J. Barroso, and E. Schamiloglu, "High-power RF generation from nonlinear transmission lines with barium titanate ceramic capacitors," *IEEE Trans. Plasma Sci.*, vol. 44, no. 12, pp. 3424–3431, Dec. 2016.
- [36] P. V. Pripitnev, I. V. Romanchenko, V. V. Rostov, O. B. Kovalchuk, and V. V. Barmin, "Nanosecond front dynamics and RF oscillation generation in a transmission line with nonlinear capacitors," in *Proc. 20th Int. Symp. High-Current Electron. (ISHCE)*, Sep. 2018, pp. 85–88.
- [37] L. R. Raimundi, J. O. Rossi, E. G. L. Rangel, L. C. Silva, E. Schamiloglu, and L. P. S. Neto, "RF generation at 200 MHz using a SiC Schottky diode lumped NLTL," in *Proc. IEEE Int. Power Modulator High Voltage Conf. (IPMHVC)*, Jun. 2018, pp. 473–476.
- [38] L. R. Raimundi, J. O. Rossi, E. G. L. Rangel, L. C. Silva, and E. Schamiloglu, "High-voltage capacitive nonlinear transmission lines for RF generation based on silicon carbide Schottky diodes," *IEEE Trans. Plasma Sci.*, vol. 47, no. 1, pp. 566–573, Jan. 2019.
- [39] L. C. Silva, J. O. Rossi, E. G. L. Rangel, L. R. Raimundi, and E. Schamiloglu, "Study of pulsed RF signal extraction and irradiation from a capacitive nonlinear transmission line," *Int. J. Adv. Eng. Res. Sci.*, vol. 5, no. 10, pp. 121–133, 2018.
- [40] L. P. S. Neto, H. M. Moraes, J. O. Rossi, J. J. Barroso, and E. G. L. Rangel, "Increasing the voltage modulation depth of the RF produced by NLTL," *IEEE Trans. Plasma Sci.*, early access, Jun. 16, 2020, doi: 10.1109/TPS.2020.3000216.
- [41] E. G. L. Rangel, J. J. Barroso, J. O. Rossi, F. S. Yamasaki, L. P. S. Neto, and E. Schamiloglu, "Influence of input pulse shape on RF generation in nonlinear transmission lines," *IEEE Trans. Plasma Sci.*, vol. 44, no. 10, pp. 2258–2267, Oct. 2016.
- [42] Y. Wang, L.-J. Lang, C. H. Lee, B. Zhang, and Y. D. Chong, "Topologically enhanced harmonic generation in a nonlinear transmission line metamaterial," *Nature Commun.*, vol. 10, no. 1, pp. 1–7, Dec. 2019.
- [43] M. Adnan and E. Afshari, "Efficient microwave and millimeter-wave frequency multipliers using nonlinear transmission lines in CMOS technology," *IEEE Trans. Microw. Theory Techn.*, vol. 63, no. 9, pp. 2889–2896, Sep. 2015.
- [44] J. B. Pendry, A. J. Holden, D. J. Robbins, and W. J. Stewart, "Magnetism from conductors and enhanced nonlinear phenomena," *IEEE Trans. Microw. Theory Techn.*, vol. 47, no. 11, pp. 2075–2084, Nov. 1999.
- [45] J. B. Pendry, "Controlling electromagnetic fields," *Science*, vol. 312, no. 5781, pp. 1780–1782, Jun. 2006.
- [46] R. Marques, F. Mesa, J. Martel, and F. Medina, "Comparative analysis of edge- and broadside-coupled split ring resonators for metamaterial design—Theory and experiments," *IEEE Trans. Antennas Propag.*, vol. 51, no. 10, pp. 2572–2581, Oct. 2003.
- [47] H. Nornikman, B. H. Ahmad, M. Z. A. A. Aziz, M. F. B. A. Malek, H. Imran, and A. R. Othman, "Study and simulation of an edge couple split ring resonator (EC-SRR) on truncated pyramidal microwave absorber," *Prog. Electromagn. Res.*, vol. 127, pp. 319–334, Apr. 2012.
- [48] F. Martin, J. Bonache, F. Falcone, M. Sorolla, and R. Marqués, "Split ring resonator-based left-handed coplanar waveguide," *Appl. Phys. Lett.*, vol. 83, no. 22, pp. 4652–4654, Dec. 2003.
- [49] V. G. Veselago, "The electrodynamics of substances with simultaneously negative values of ϵ and μ ," *Sov. Phys. Uspekhi*, vol. 10, no. 4, pp. 509–514, Apr. 1968.
- [50] W. Tang, G. Goussetis, N. J. G. Fonseca, H. Legay, E. Saenz, and P. de Maagt, "Coupled split-ring resonator circular polarization selective surface," *IEEE Trans. Antennas Propag.*, vol. 65, no. 9, pp. 4664–4675, Sep. 2017.
- [51] A. Rigi-Tamandani, J. Ahmadi-Shokouh, and S. Tavakoli, "Wideband planar split ring resonator based metamaterials," *Prog. Electromagn. Res. M*, vol. 28, pp. 115–128, Jan. 2013.
- [52] T. J. Cui, D. Smith, and R. Liu, *Metamaterials Theory, Design, and Applications*. Boston, MA, USA: Springer, 2010.
- [53] M. Shamonin, E. Shamonina, V. Kalinin, and L. Solymar, "Resonant frequencies of a split-ring resonator: Analytical solutions and numerical simulations," *Microw. Opt. Technol. Lett.*, vol. 44, no. 2, pp. 133–136, Jan. 2005.
- [54] B. Sauviac, C. R. Simovski, and S. A. Tretyakov, "Double split-ring resonators: Analytical modeling and numerical simulations," *Electromagnetics*, vol. 24, no. 5, pp. 317–338, Jan. 2004.
- [55] O. Sydoruk, E. Tatartschuk, E. Shamonina, and L. Solymar, "Analytical formulation for the resonant frequency of split rings," *J. Appl. Phys.*, vol. 105, no. 1, Jan. 2009, Art. no. 014903.
- [56] J. D. Baena, J. Bonache, F. Martin, R. M. Sillero, F. Falcone, T. Lopetegui, M. A. G. Laso, J. Garcia-Garcia, I. Gil, M. F. Portillo, and M. Sorolla, "Equivalent-circuit models for split-ring resonators and complementary split-ring resonators coupled to planar transmission lines," *IEEE Trans. Microw. Theory Techn.*, vol. 53, no. 4, pp. 1451–1461, Apr. 2005.
- [57] F. Qureshi, M. A. Antoniadou, and G. V. Eleftheriades, "A compact and low-profile metamaterial ring antenna with vertical polarization," *IEEE Antennas Wireless Propag. Lett.*, vol. 4, pp. 333–336, 2005.
- [58] M. A. Rahman, M. R. I. Faruque, and M. T. Islam, "Circularly split-ring-resonator-based frequency-reconfigurable antenna," *Appl. Phys. A, Solids Surf.*, vol. 123, no. 1, p. 110, Jan. 2017.
- [59] S. I. Maslovski, P. M. T. Ikonen, I. Kolmakov, S. A. Tretyakov, and M. Kaunisto, "Artificial magnetic materials based on the new magnetic particle: Metasolenoid," *Prog. Electromagn. Res.*, vol. 54, pp. 61–81, Jan. 2005.
- [60] R. Liu, T. J. Cui, D. Huang, B. Zhao, and D. R. Smith, "Description and explanation of electromagnetic behaviors in artificial metamaterials based on effective medium theory," *Phys. Rev. E, Stat. Phys. Plasmas Fluids Relat. Interdiscip. Top.*, vol. 76, no. 2, Aug. 2007, Art. no. 026606.
- [61] F. Bilotti, A. Toscano, L. Vegni, K. B. Alici, and E. Ozbay, "Equivalent-circuit models for the design of metamaterials based on artificial magnetic inclusions," *IEEE Trans. Microw. Theory Techn.*, vol. 55, no. 12, pp. 2865–2873, Dec. 2007.
- [62] A. Kabiri, L. Yousefi, and O. M. Ramahi, "On the fundamental limitations of artificial magnetic materials," *IEEE Trans. Antennas Propag.*, vol. 58, no. 7, pp. 2345–2353, Jul. 2010.
- [63] E. Poutrina, D. Huang, and D. R. Smith, "Analysis of nonlinear electromagnetic metamaterials," *New J. Phys.*, vol. 12, no. 9, Sep. 2010, Art. no. 093010.
- [64] K. Payandehjoo and R. Abhari, "Suppression of unwanted harmonics using integrated complementary split-ring resonators in nonlinear transmission line frequency multipliers," *IEEE Trans. Microw. Theory Techn.*, vol. 56, no. 4, pp. 931–941, Apr. 2008.
- [65] Z. Duan, J. S. Hummelt, M. A. Shapiro, and R. J. Temkin, "Sub-wavelength waveguide loaded by a complementary electric metamaterial for vacuum electron devices," *Phys. Plasmas*, vol. 21, no. 10, Oct. 2014, Art. no. 103301.
- [66] D. M. French, D. Shiffler, and K. Cartwright, "Electron beam coupling to a metamaterial structure," *Phys. Plasmas*, vol. 20, no. 8, Aug. 2013, Art. no. 083116.
- [67] D. Shiffler, R. Seviour, E. Luchinskaya, E. Stranford, W. Tang, and D. French, "Study of split-ring resonators as a metamaterial for high-power microwave power transmission and the role of defects," *IEEE Trans. Plasma Sci.*, vol. 41, no. 6, pp. 1679–1685, Jun. 2013.
- [68] J. A. Bossard, C. P. Scarborough, Q. Wu, S. D. Campbell, D. H. Werner, P. L. Werner, S. Griffiths, and M. Ketner, "Mitigating field enhancement in metasurfaces and metamaterials for high-power microwave applications," *IEEE Trans. Antennas Propag.*, vol. 64, no. 12, pp. 5309–5319, Dec. 2016.
- [69] D. R. Smith, W. J. Padilla, D. C. Vier, S. C. Nemat-Nasser, and S. Schultz, "Composite medium with simultaneously negative permeability and permittivity," *Phys. Rev. Lett.*, vol. 84, no. 18, pp. 4184–4187, May 2000.

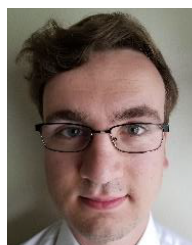
- [70] D. R. Smith, S. Schultz, P. Markoš, and C. M. Soukoulis, "Determination of effective permittivity and permeability of metamaterials from reflection and transmission coefficients," *Phys. Rev. B, Condens. Matter*, vol. 65, no. 19, Apr. 2002, Art. no. 195104.
- [71] D. Bensafieddine, F. Djerfaj, F. Chouireb, and D. Vincent, "Design of tunable microwave transmission lines using metamaterial cells," *Appl. Phys. A, Solids Surf.*, vol. 123, no. 4, p. 248, Apr. 2017.
- [72] K. Aydin and E. Ozbay, "Capacitor-loaded split ring resonators as tunable metamaterial components," *J. Appl. Phys.*, vol. 101, no. 2, Jan. 2007, Art. no. 024911.
- [73] K. Aydin, A. O. Cakmak, L. Sahin, Z. Li, F. Bilotti, L. Vegni, and E. Ozbay, "Split-ring-resonator-coupled enhanced transmission through a single subwavelength aperture," *Phys. Rev. Lett.*, vol. 102, no. 1, Jan. 2009.
- [74] T. Okamoto, T. Otsuka, S. Sato, T. Fukuta, and M. Haraguchi, "Dependence of LC resonance wavelength on size of silver split-ring resonator fabricated by nanosphere lithography," *Opt. Express*, vol. 20, no. 21, p. 24059, Oct. 2012.
- [75] L.-C. Tsai and W.-J. Chen, "A UWB antenna with band-notched filters using slot-type split ring resonators," *Microw. Opt. Technol. Lett.*, vol. 58, no. 11, pp. 2595–2598, Nov. 2016.
- [76] R. Seviour, Y. S. Tan, and A. Hopper, "Effects of high power on microwave metamaterials," in *Proc. 8th Int. Congr. Adv. Electromagn. Mater. Microw. Opt.*, Aug. 2014, pp. 142–144.
- [77] E. G. L. Rangel, J. O. Rossi, J. J. Barroso, F. S. Yamasaki, and E. Schamiloglu, "Practical constraints on nonlinear transmission lines for RF generation," *IEEE Trans. Plasma Sci.*, vol. 47, no. 1, pp. 1000–1016, Jan. 2019.
- [78] E. M. Gyorgy, "Rotational model of flux reversal in square loop ferrites," *J. Appl. Phys.*, vol. 28, no. 9, pp. 1011–1015, Sep. 1957.
- [79] H. C. Hsieh, "Coupled mode theory in a lossy, nonlinear transmission line system," *J. Appl. Phys.*, vol. 62, no. 5, pp. 2095–2102, Sep. 1987.
- [80] E. Sawado, M. Taki, and S. Kiliu, "Nonlinear magnetic lattice and the modified Korteweg-de Vries equation," *Phys. Rev. B, Condens. Matter*, vol. 38, no. 16, pp. 11911–11914, Dec. 1988.
- [81] H. Ikezi, S. S. Wojtowicz, R. E. Waltz, J. S. DeGrassie, and D. R. Baker, "High-power soliton generation at microwave frequencies," *J. Appl. Phys.*, vol. 64, no. 6, pp. 3277–3281, Sep. 1988.
- [82] R. Luebbers, K. Kumagai, S. Adachi, and T. Uno, "FDTD calculation of transient pulse propagation through a nonlinear magnetic sheet," *IEEE Trans. Electromagn. Compat.*, vol. 35, no. 1, pp. 90–94, Feb. 1993.
- [83] M. P. Brown, "High voltage soliton production in nonlinear transmission lines and other pulsed power applications," Ph.D. dissertation, Oriol College, Univ. Oxford, Oxford, U.K., 1997.
- [84] F. Crowne, "Modeling and simulation of nonlinear dynamics," Army Res. Lab. Adelphi, MD, USA, Tech. Rep. ARL-TR-5062, Jan. 2010.
- [85] E. Gluskin, "A nonlinear resistor and nonlinear inductor using a nonlinear capacitor," *J. Franklin Inst.*, vol. 336, no. 7, pp. 1035–1047, Sep. 1999.
- [86] L. Gao, X. Yang, J. Hu, and J. He, "ZnO microvaristors doped polymer composites with electrical field dependent nonlinear conductive and dielectric characteristics," *Mater. Lett.*, vol. 171, pp. 1–4, May 2016.
- [87] V. G. Harris, "Modern microwave ferrites," *IEEE Trans. Magn.*, vol. 48, no. 3, pp. 1075–1104, Mar. 2012.
- [88] F. Qin and H.-X. Peng, "Ferromagnetic microwires enabled multifunctional composite materials," *Prog. Mater. Sci.*, vol. 58, no. 2, pp. 183–259, Mar. 2013.
- [89] G. Zhao, R. P. Joshi, S. Rogers, E. Schamiloglu, and H. P. Hjalmarson, "Simulation studies for nonlinear-transmission-line based ultrafast rise times and waveform shaping for pulsed-power applications," *IEEE Trans. Plasma Sci.*, vol. 36, no. 5, pp. 2618–2625, Oct. 2008.
- [90] H. A. Ávila, M. M. Reboredo, R. Parra, and M. S. Castro, "Dielectric permittivity calculation of composites based on electrospun barium titanate fibers," *Mater. Res. Exp.*, vol. 2, no. 4, Apr. 2015, Art. no. 045302.
- [91] K. A. O'Connor and R. D. Curry, "Three-dimensional electromagnetic modeling of composite dielectric materials," in *Proc. IEEE Pulsed Power Conf.*, Jun. 2011, pp. 274–279.
- [92] A. L. Garner, G. J. Parker, and D. L. Simone, "A semi-empirical approach for predicting the performance of multiphase composites at microwave frequencies," *IEEE Trans. Dielectr. Electr. Insul.*, vol. 23, no. 2, pp. 1126–1134, Apr. 2016.
- [93] A. L. Garner, G. J. Parker, and D. L. Simone, "Accounting for conducting inclusion permeability in the microwave regime in a modified generalized effective medium theory," *IEEE Trans. Dielectr. Electr. Insul.*, vol. 22, no. 4, pp. 2064–2072, Aug. 2015.
- [94] M. Lapine, I. V. Shadrivov, and Y. S. Kivshar, "Colloquium: Nonlinear metamaterials," *Rev. Mod. Phys.*, vol. 86, no. 3, pp. 1093–1123, Sep. 2014.
- [95] M. Y. Koledintseva, R. E. DuBroff, R. W. Schwartz, and J. L. Drewniak, "Double statistical distribution of conductivity and aspect ratio of inclusions in dielectric mixtures at microwave frequencies," *Prog. Electromagn. Res.*, vol. 77, pp. 193–214, Jun. 2007.
- [96] B. A. Slovick, Z. G. Yu, and S. Krishnamurthy, "Generalized effective-medium theory for metamaterials," *Phys. Rev. B, Condens. Matter*, vol. 89, no. 15, Apr. 2014, Art. no. 155118.
- [97] Z. Szabo and J. Fuzi, "Equivalence of magnetic metamaterials and composites in the view of effective medium theories," *IEEE Trans. Magn.*, vol. 50, no. 4, pp. 1–4, Apr. 2014.
- [98] E. Kengne and W. M. Liu, "Exact solutions of the derivative nonlinear Schrödinger equation for a nonlinear transmission line," *Phys. Rev. E, Stat. Phys. Plasmas Fluids Relat. Interdiscip. Top.*, vol. 73, no. 2, Feb. 2006, Art. no. 026603.
- [99] I. V. Romanchenko and V. V. Rostov, "Energy levels of oscillations in a nonlinear transmission line filled with saturated ferrite," *Tech. Phys.*, vol. 55, no. 7, pp. 1024–1027, Jul. 2010.
- [100] F. S. Yamasaki, E. Schamiloglu, J. O. Rossi, and J. J. Barroso, "Simulation studies of distributed nonlinear gyromagnetic lines based on LC lumped model," *IEEE Trans. Plasma Sci.*, vol. 44, no. 10, pp. 2232–2239, Oct. 2016.
- [101] T. L. Gilbert, "A phenomenological theory of damping in ferromagnetic materials," *IEEE Trans. Magn.*, vol. 40, no. 6, pp. 3443–3449, Nov. 2004.
- [102] S. Y. Karelin, V. B. Krasovitsky, I. I. Magda, V. S. Mukhin, and V. G. Sinitin, "Radio frequency oscillations in gyrotropic nonlinear transmission lines," *Plasma*, vol. 2, no. 2, pp. 258–271, Jun. 2019.
- [103] I. G. Kataev, *Electromagnetic Shock Waves*. London, U.K.: Iiffee Books, 1966.
- [104] G. Branch and P. W. Smith, "Shock waves in transmission lines with nonlinear dielectrics," in *Proc. IEE Colloq. Pulsed Power*, 1993, pp. 7-1–7-3.
- [105] S. N. Rukin, "Pulsed power technology based on semiconductor opening switches: A review," *Rev. Sci. Instrum.*, vol. 91, no. 1, Jan. 2020, Art. no. 011501.
- [106] A. I. Gusev, M. S. Pedos, A. V. Ponomarev, S. N. Rukin, S. P. Timoshenkov, and S. N. Tsyranov, "A 30 GW subnanosecond solid-state pulsed power system based on generator with semiconductor opening switch and gyromagnetic nonlinear transmission lines," *Rev. Sci. Instrum.*, vol. 89, no. 9, Sep. 2018, Art. no. 094703.
- [107] W. Tie, C. Meng, C. Zhao, X. Lu, J. Xie, D. Jiang, and Z. Yan, "Optimized analysis of sharpening characteristics of a compact RF pulse source based on a gyro-magnetic nonlinear transmission line for ultrawideband electromagnetic pulse application," *Plasma Sci. Technol.*, vol. 21, no. 9, Sep. 2019, Art. no. 095503.
- [108] M. R. Ulmaskulov, S. A. Shunailov, K. A. Sharypov, and M. I. Yalandin, "Multistage converter of high-voltage subnanosecond pulses based on nonlinear transmission lines," *J. Appl. Phys.*, vol. 126, no. 8, Aug. 2019, Art. no. 084504.
- [109] J.-W.-B. Bragg, W. W. Sullivan, D. Mauch, A. A. Neuber, and J. C. Dickens, "All solid-state high power microwave source with high repetition frequency," *Rev. Sci. Instrum.*, vol. 84, no. 5, May 2013, Art. no. 054703.
- [110] J.-W.-B. Bragg, J. C. Dickens, and A. A. Neuber, "Material selection considerations for coaxial, ferrimagnetic-based nonlinear transmission lines," *J. Appl. Phys.*, vol. 113, no. 6, Feb. 2013, Art. no. 064904.
- [111] D. M. French and B. W. Hoff, "Spatially dispersive ferrite nonlinear transmission line with axial bias," *IEEE Trans. Plasma Sci.*, vol. 42, no. 10, pp. 3387–3390, Oct. 2014.
- [112] D. V. Reale, J.-W.-B. Bragg, N. R. Gonsalves, J. M. Johnson, A. A. Neuber, J. C. Dickens, and J. J. Mankowski, "Bias-field controlled phasing and power combination of gyromagnetic nonlinear transmission lines," *Rev. Sci. Instrum.*, vol. 85, no. 5, May 2014, Art. no. 054706.
- [113] J. M. Johnson, D. V. Reale, W. H. Cravey, R. S. Garcia, D. H. Barnett, A. A. Neuber, J. C. Dickens, and J. J. Mankowski, "Material selection of a ferrimagnetic loaded coaxial delay line for phasing gyromagnetic nonlinear transmission lines," *Rev. Sci. Instrum.*, vol. 86, no. 8, Aug. 2015, Art. no. 084702.
- [114] I. V. Romanchenko, V. V. Rostov, A. V. Gunin, and V. Y. Konev, "High power microwave beam steering based on gyromagnetic nonlinear transmission lines," *J. Appl. Phys.*, vol. 117, no. 21, Jun. 2015, Art. no. 214907.

- [115] J. M. Johnson, D. V. Reale, J. T. Krile, R. S. Garcia, W. H. Cravey, A. A. Neuber, J. C. Dickens, and J. J. Mankowski, "Characteristics of a four element gyromagnetic nonlinear transmission line array high power microwave source," *Rev. Sci. Instrum.*, vol. 87, no. 5, May 2016, Art. no. 054704.
- [116] M. R. Ul'maskulov, S. A. Shunailov, K. A. Sharypov, M. I. Yalandin, V. G. Shpak, M. S. Pedos, and S. N. Rukin, "Coherent summation of radiation from four-channel shock-excited RF source operating at 4 GHz and a repetition rate of 1000 Hz," *IEEE Trans. Plasma Sci.*, vol. 45, no. 10, pp. 2623–2628, Oct. 2017.
- [117] M. R. Ulmaskulov, S. A. Shunailov, K. A. Sharypov, M. I. Yalandin, V. G. Shpak, S. N. Rukin, and M. S. Pedos, "Four-channel generator of 8-GHz radiation based on gyromagnetic non-linear transmitting lines," *Rev. Sci. Instrum.*, vol. 90, no. 6, Jun. 2019, Art. no. 064703.
- [118] I. V. Romanchenko, M. R. Ulmaskulov, K. A. Sharypov, S. A. Shunailov, V. G. Shpak, M. I. Yalandin, M. S. Pedos, S. N. Rukin, V. Y. Konev, and V. V. Rostov, "Four channel high power RF source with beam steering based on gyromagnetic nonlinear transmission lines," *Rev. Sci. Instrum.*, vol. 88, no. 5, May 2017, Art. no. 054703.
- [119] K. M. Noel, A. M. Pearson, R. D. Curry, and K. A. O'Connor, "High frequency properties of high voltage barium titanate-ferrite multiferroic metamaterial composites," *IEEE Trans. Dielectr. Electr. Insul.*, vol. 23, no. 5, pp. 2965–2969, Oct. 2016.
- [120] D. V. Reale, J. M. Parson, A. A. Neuber, J. C. Dickens, and J. J. Mankowski, "Investigation of a stripline transmission line structure for gyromagnetic nonlinear transmission line high power microwave sources," *Rev. Sci. Instrum.*, vol. 87, no. 3, Mar. 2016, Art. no. 034706.
- [121] Q. J. Li, Z. P. Zhang, W. Ni, X. H. Sun, and C. C. Wang, "Large and switchable dielectric tunability in $\text{Na}_{1/2}\text{Bi}_{1/2}\text{Cu}_3\text{Ti}_4\text{O}_{12}$ ceramics," *J. Alloys Compounds*, vol. 695, pp. 1561–1565, Feb. 2017.
- [122] R. Gholipur and A. Bahari, "Effect of electric field on the dielectric and magnetic properties of random nanocomposites," *Mater. Des.*, vol. 94, pp. 139–147, Mar. 2016.
- [123] I. V. Romanchenko, V. V. Rostov, A. V. Gunin, and V. Y. Konev, "Gyro-magnetic RF source for interdisciplinary research," *Rev. Sci. Instrum.*, vol. 88, no. 2, Feb. 2017, Art. no. 024703.
- [124] A. I. Gusev, M. S. Pedos, S. N. Rukin, and S. P. Timoshenkov, "Solid-state repetitive generator with a gyromagnetic nonlinear transmission line operating as a peak power amplifier," *Rev. Sci. Instrum.*, vol. 88, no. 7, Jul. 2017, Art. no. 074703.
- [125] B. W. Hoff, D. M. French, D. S. Simon, P. D. Lepell, T. Montoya, and S. L. Heidger, "High current nonlinear transmission line based electron beam driver," *Phys. Rev. A, Gen. Phys.*, vol. 20, no. 10, Oct. 2017.
- [126] B. W. Hoff and D. M. French, "Simulations of a disk-on-rod TWT driven by an NLTL-modulated electron beam," *IEEE Trans. Plasma Sci.*, vol. 44, no. 8, pp. 1265–1269, Aug. 2016.
- [127] J. A. Schrock, B. W. Hoff, D. H. Simon, S. L. Heidger, P. Lepell, J. Gilbrech, H. Wood, and R. Richter-Sand, "Spatially dispersive nonlinear transmission line experimental performance analysis," *IEEE Trans. Dielectr. Electr. Insul.*, vol. 26, no. 2, pp. 412–415, Apr. 2019.
- [128] J. O. Rossi and P. N. Rizzo, "Study of hybrid nonlinear transmission lines for high power RF generation," in *Proc. IEEE Pulsed Power Conf.*, Jun. 2009, pp. 46–50.
- [129] L. P. S. Neto, J. O. Rossi, J. J. Barroso, and E. Schamiloglu, "Hybrid nonlinear transmission lines used for RF soliton generation," *IEEE Trans. Plasma Sci.*, vol. 46, no. 10, pp. 3648–3652, Oct. 2018.
- [130] J. O. Rossi, P. N. Rizzo, and F. S. Yamasaki, "Prospects for applications of hybrid lines in RF generation," in *Proc. IEEE Int. Power Modulator High Voltage Conf.*, May 2010, pp. 632–635.
- [131] P. V. Pripitnev, I. V. Romanchenko, P. V. Vykhodtsev, S. N. Maltsev, and V. Y. Konev, "RF pulse generation in combined nonlinear gyromagnetic transmission line," in *Proc. Int. Multi-Conf. Eng., Comput. Inf. Sci. (SIBIRCON)*, Oct. 2019, pp. 0261–0264.
- [132] M. S. Nikoo, S. M.-A. Hashemi, and F. Farzaneh, "Theoretical analysis of RF pulse termination in nonlinear transmission lines," *IEEE Trans. Microw. Theory Techn.*, vol. 66, no. 1, pp. 4757–4764, Nov. 2018.



energy, microscale breakdown, and electroporation.

ANDREW J. FAIRBANKS (Graduate Student Member, IEEE) received the B.S. and M.S. degrees in nuclear engineering from Purdue University, West Lafayette, IN, USA, in 2015 and 2017, respectively. He is currently pursuing the Ph.D. degree in nuclear engineering with the Bio-Electrics and ElectroPhysics Laboratory, School of Nuclear Engineering, Purdue University, West Lafayette, IN, USA. His research interests include high-power microwaves, pulsed power, directed



ADAM M. DARR (Graduate Student Member, IEEE) received the B.S. degree in nuclear engineering from Purdue University, West Lafayette, IN, USA. He is currently pursuing the Ph.D. degree in nuclear engineering with the Bioelectrics and Electrophysics Laboratory, Purdue University, West Lafayette, IN, USA. His research interests include micro- and nanoscale field, thermal, photo-, and space-charge limited emission, and electroporation.



ALLEN L. GARNER (Senior Member, IEEE) received the B.S. degree (Hons.) in nuclear engineering from the University of Illinois at Urbana-Champaign, in 1996, the M.S.E. degree in nuclear engineering from the University of Michigan, Ann Arbor, in 1997, the M.S. degree in electrical engineering from Old Dominion University, Norfolk, VA, USA, in 2003, and the Ph.D. degree in nuclear engineering from the University of Michigan, in 2006.

From December 1997 to December 2003, he was an active duty Naval Officer serving onboard the USS Pasadena (SSN 752). He was also an Instructor with the Prospective Nuclear Engineering Officer Course, Submarine Training Facility, Norfolk. From 2006 to 2012, he was an Electromagnetic Physicist with GE Global Research Center, Niskayuna, NY, USA. In August 2012, he joined the School of Nuclear Engineering, Purdue University, West Lafayette, IN, USA, where he is currently an Associate Professor and the Undergraduate Program Chair. He is also a Captain with the Navy Reserves and a Commanding Officer with the ONR S&T 102 Unit, Washington, DC, USA. His research interests include electron emission, gas breakdown, high-power microwaves, and biomedical applications of pulsed power and plasmas.

Dr. Garner is a member of the IEEE International Power Modulator and High Voltage Conference (IPMHVC) Executive Committee and the Dielectrics and Electrical Insulation Society Administrative Committee. He received the 2016 IEEE Nuclear and Plasma Sciences Early Achievement Award, two Meritorious Service Medals, the Navy and Marine Corps Commendation Medal, and five Navy and Marine Corps Achievement Medals. He served as the Technical Program Chair for the 2016 IEEE IPMHVC and a Treasurer for the 2018 IEEE IPMHVC. He is a Licensed Professional Engineer, Michigan.

• • •